# Dynamics of a tightly coupled mechanism for flagellar rotation

## Bacterial motility, chemiosmotic coupling, protonmotive force

Markus Meister,* S. Roy Caplan,‡ and Howard C. Berg§

*Department of Neurobiology, Stanford University School of Medicine, Stanford, California 94305; ‡Department of Membrane Research, The Weizmann Institute of Science, 76100 Rehovot, Israel; and §Department of Cellular and Developmental Biology, Harvard University, Cambridge, Massachusetts 02138, and The Rowland Institute for Science, Cambridge, Massachusetts 02142

ABSTRACT The bacterial flagellar motor is a molecular engine that couples the flow of protons across the cytoplasmic membrane to rotation of the flagellar filament. We analyze the steady-state behavior of an explicit mechanical model in which a fixed number of protons carries the filament through one revolution. Predictions of this model are compared with experimentally determined relationships between protonmotive force, proton flux, torque, and speed. All such tightly coupled mechanisms produce the same torque when the motor is stalled but vary greatly in their behavior at high speed. The speed at zero load predicted by our model is limited by the rates of association and dissociation of protons at binding sites on the rotor and by the mobility of force generators containing transmembrane channels that interact with these sites. Our analysis suggests that more could be learned about the motor if it were driven by an externally applied torque backwards (at negative speed) or forwards at speeds greater than the zero-load speed.

## INTRODUCTION

Flagellated bacteria are propelled by thin helical filaments, each driven at its base by a rotary motor (Berg and Anderson, 1973; Silverman and Simon, 1974). The direction of rotation of these filaments determines the manner in which a cell swims. Directional control is imposed by sensory systems sensitive to a variety of inputs, such as the concentration of chemicals in the cell's environment, temperature, or intensity of light. The system that has been studied most extensively processes chemical stimuli. For recent reviews on chemotaxis in *Escherichia coli* and *Salmonella typhimurium*, see Macnab (1987*a*) and Stewart and Dahlquist (1987). The flagellar motor is comprised of at least two rings with a diameter of ~25 nm mounted on a rod that connects to the helical filament. One of these rings, the M-ring, lies in the plane of the cytoplasmic membrane (DePamphilis and Adler, 1971) and is thought to be attached rigidly to the rotating rod (Berg, 1974). It is surrounded by a circlet of membrane particles (Coulton and Murray, 1978; Khan et al., 1988) that appear to act as independent force-generating units (Block and Berg, 1984; Blair and Berg, 1988). Flagellar motility is driven by a transmembrane flux of protons (or, in some alkalophilic or marine organisms, of sodium ions); ATP is not required. For recent reviews on motor structure and function, see Berg et al. (1982), Macnab and Aizawa (1984), and Macnab (1987*b*).

Two methods for monitoring flagellar rotation have proved particularly useful. In the first, a bacterium is tethered to a glass surface by one of its flagellar filaments (Silverman and Simon, 1974). Operation of the motor at the base of this filament generates rotation of the cell body, which is easily observed by light microscopy. These cells rotate at rates of up to ~15 Hz. The torque driving the rotation can be calculated from the rotational drag coefficient of the cell body (Meister and Berg, 1987). In the second method, images of swimming cells are focussed on a photomultiplier tube, and the vibration frequencies of the cell bodies are determined by Fourier analysis of its output signal; higher-frequency components are due to rotation of the flagellar bundles (Lowe et al., 1987). The drag coefficient of an individual filament in a bundle is relatively small, so the motors of swimming cells rotate at high speeds, on the order of 100 Hz (at room temperature). The torque driving this rotation can be calculated from the drag coefficient of the counter-rotating cell body and the number of filaments in the bundle. These measurements enable one to determine the power output of the flagellar motor, the product of torque and speed. The protonmotive force across the cytoplasmic membrane can be measured by a variety of established techniques (reviewed by Kashket, 1985) and set by manipulating potassium diffusion potentials or pH gradients. The rotation-dependent proton flux can be measured in a suspension of swimming cells by monitoring the drop in the total transmembrane proton flux that occurs when motility is blocked by the addition of anti-filament antibody (Meister et al., 1987). Assuming that this constitutes the entire flux of protons through the motor, one can determine the power input to the motor, the product of proton flux and protonmotive force.

Here we discuss a hypothetical mechanism for energy conversion in which flagellar rotation is tightly coupled to

proton flux. This mechanism has been described before, but its behavior has been analyzed only for the relatively low rotation rates accessible with tethered cells (Berg and Khan, 1983; Khan and Berg, 1983). In this regime, all mechanisms in which rotation of the filament is tightly coupled to proton flux make identical predictions for the torque. Models within this class can be distinguished only by observations made at high speeds, which are now becoming available. We will consider two processes that might determine the motor's performance at the high rotation rates found in swimming cells: the transfer of protons to and from proton binding sites within the motor and the mechanical movement of its internal components.

## A MODEL FOR THE FLAGELLAR MOTOR

Our recent experimental effort has been guided by a model for the rotary motor in which a number of independent force generators interact with the periphery of the M-ring and provide the coupling between proton movement and rotation of the filament. Fig. 1 shows the components of this model mechanism. The rotor consists of the M-ring, which is rigidly connected to the rod and immersed in the cytoplasmic membrane. It carries a set of identical proton-accepting sites, spaced equidistantly on its periphery. Protons from the cytoplasm or the extracellular medium gain access to those sites only by moving through adjacent transmembrane particles called channel complexes. These devices form part of the stator. They span the membrane and are connected to the cell wall by elastic linkages which allow them to move in close proximity to the periphery of the rotor. Each channel complex contains two half-channels that run perpendicularly to the plane of the membrane and are separated by the same distance as the proton-accepting sites. When a pair of adjacent sites on the rotor is aligned with the two half-channels of a channel complex, one of the sites (the *i*-site) is in contact with the cytoplasm (inner medium), while the other site (the *o*-site) is in contact with the extracellular (or outer) medium. Thus, the occupancies of the two sites will depend on the proton concentrations at the internal and external faces of the membrane, as well as on the difference in electrical potential across the membrane.

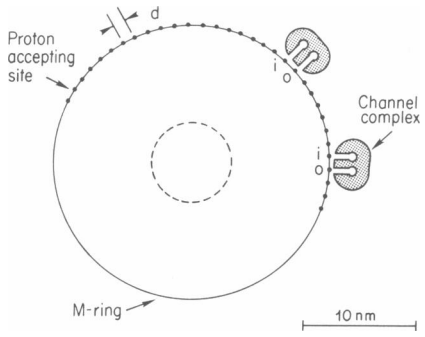


FIGURE 1 Components of the motor mechanism. The M-ring and two of the force generators (channel complexes) are shown in a section cut parallel to the plane of the cytoplasmic membrane. The intersection between the ring and the rod is indicated by the dashed circle. A set of identical proton-accepting sites are spaced equidistantly on the periphery of the M-ring: *i* refers to a site adjacent to a half channel leading to the inner surface of the cytoplasmic membrane; *o* refers to a site adjacent to a half channel leading to the outer surface of the cytoplasmic membrane. The channel complexes are linked elastically to the rigid framework of the cell wall (connections not shown).

Motion of the channel complex relative to the rotor is subject to the following constraints: the ends of the complex cannot move past a proton-accepting (or -binding) site if that site is occupied, and the center of the complex cannot move past such a site if that site is empty. Fig. 2 illustrates how these constraints lead to coupling between proton translocation and rotation of the filament. In Fig. 2 *a* the complex is free to move to the right but not to the left. If thermal motion carries it one step to the right, as shown in Fig. 2 *b*, the proton on the binding site can move into the cytoplasm, whereas another proton from the extracellular medium can move onto the adjacent empty binding site. This leads to the state shown in Fig. 2 *c*. The cycle is completed when the M-ring rotates under the force exerted by the elastic linkage of the channel complex, returning the system to the state shown in Fig. 2 *a*. These coupling constraints are assumed to be absolutely tight, allowing no slip between proton translocation across the membrane and movement of the channel complex relative to the rotor. This implies that during steady rotation of the filament, each channel complex transfers a constant number of protons per revolution, which is equal to the number of binding sites on the M-ring.

The bacterial motor is known to reverse its sense of rotation without changing the direction of proton transfer. In this model, reverse rotation can be achieved by inverting the constraints that limit the motion of each channel complex. For example, the M-ring might bend (moving its periphery in a direction normal to the plane of the membrane) in such a way as to bring a new set of proton-accepting sites into register with each half-channel. Assume that it is charge rather than occupancy that determines the constraints. Then if one set of sites became positively charged on accepting a proton and the other set became neutral (as would happen, for example, if the first set comprised imidazole groups and the second carboxyl groups), the direction of movement of the channel complex relative to the rotor would change when the sets of sites changed. Because the arguments about force genera-

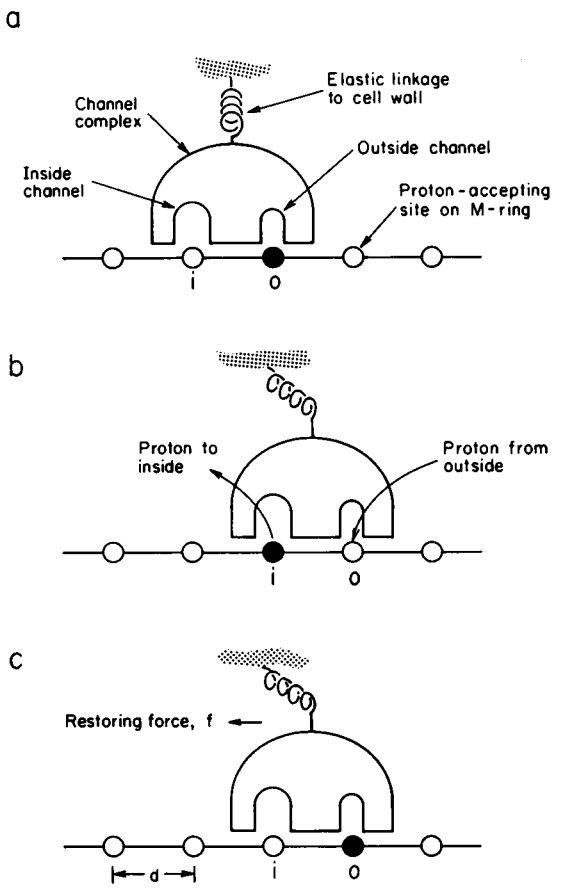


FIGURE 2 Coupling between rotation of the filament and proton translocation. A channel complex is shown schematically interacting with two of five proton-accepting sites at the periphery of the M-ring. The perspective is the same as that in Fig. 1. (*a*) Site *o* is occupied and site *i* is empty, and the complex is free to move to the right. If thermal motion carries it one step to the right, as shown in *b*, the proton on the occupied site can move into the cytoplasm, while a proton from the external medium can move onto the adjacent empty site. This brings the complex to the state shown in *c*, which is identical to *a* except for a displacement by the distance *d*.

tion are the same in either case, we will not consider this complication further.

If a proton gradient is imposed across the membrane, such that the concentration of protons at the *o*-site exceeds that at the *i*-site, the channel complex will step to the right more often than to the left (Fig. 2). One can view its motion as a thermal walk among the sites on the rotor, biased by the protonmotive force and by the restoring force in the elastic linkage between the channel complex and the cell wall. If the rotor is held rigidly fixed by applying external torque to the filament (a condition that we call "stall"), the channel complex will advance, stretching the elastic linkage until the bias due to its restoring force just balances that due to the protonmotive force. At this point, the net stepping rate will vanish. If the rotor is allowed to turn under the force exerted by the elastic linkage, a steady state will be reached when the complex steps forward along the rotor at a net rate that just compensates for the backward motion of the binding sites. To achieve this, the elastic linkage must be relaxed relative to the stalled case, leaving the random walk with a net forward bias. Thus, the torque generated by the rotating motor will be lower than the stall torque. Note that several channel complexes can operate independently along the periphery of the rotor. If so, the sum of the forces in all of their elastic linkages will determine the torque generated by the motor. In the treatment that follows, our object is to calculate the net stepping rate of the channel complex as a function of the protonmotive force and the force in the elastic linkage. This will yield the relationship between protonmotive force, torque, and speed of the motor.

A quantitative analysis requires more detailed assumptions about the properties of the channel complex. We assume that the conductances of the channels are so large that they never limit the proton flux through the motor. Under these conditions, the channels act as proton wells, transforming an electric potential difference across the membrane into a thermodynamically equivalent proton concentration difference at the two proton-binding sites. If these sites are separated from the cytoplasm by a fraction $\chi$ of the total transmembrane electrical distance, the proton activities at the *i*-site, $H_i$, and at the *o*-site, $H_o$, are given by

$$H_o = H_i \exp(-e\Delta p/kT), \text{ and} \tag{1}$$

$$H_i = H_{in} \exp(\chi e\Delta\psi/kT), \tag{2}$$

where $e$ is the charge on the proton,

$$\Delta p = (kT/e)\, ln\, (H_{in}/H_{out}) + \Delta\psi$$

is the protonmotive force, $\Delta\psi$ is the electrical potential of the inner medium less that of the outer medium, and $H_{in}$ and $H_{out}$ are the proton concentrations in the inner and outer media, respectively. Note that if $\chi = 0$, as assumed before (Berg and Khan, 1983), the pH at the *i*-site is equal to the cytoplasmic pH, and the sole effect of $\Delta\psi$ is a pH change at the *o*-site.

To pass through the motor, protons must bind to a proton-accepting site at the bottom of one channel and leave that site when it is adjacent to the bottom of the other channel. These processes are taken to occur at finite rates. An empty *o*-site is protonated at the rate

$$k_{o+} = hH_o, \tag{3}$$

where $h$ is the bimolecular rate constant for association of protons with the binding sites. An empty *i*-site is proton-

ated at the rate

$$k_{i+} = hH_i. \tag{4}$$

An occupied $i$-site or $o$-site releases its proton at the rate

$$k_{-} = hK, \tag{5}$$

where $K$ is the site's dissociation constant.

We will treat the motion of the channel complex along the M-ring as a series of instantaneous steps between adjacent positions of alignment with a pair of proton-accepting sites—see Meister (1987) for an alternative analysis, in which the channel complex performs continuous Brownian motion along the periphery of the M-ring. This choice of reducing a continuous coordinate to a set of discrete states simplifies the formalism and is frequently made in treating the dynamics of a macromolecular system, often without a priori evidence for the existence of such states. It implies the physical assumption that the free energy of the system varies strongly along that particular coordinate, and that the discrete states represent valleys in the free energy diagram separated by barriers which are large compared to $kT$. In our case, we will assume that these potential barriers result from interactions between the channel complex and the M-ring. In addition, the channel complex experiences the force in its elastic linkage to the stator. Fig. 3 illustrates the combined potential affecting the motion of the channel complex. With these assumptions, steps of the channel complex between adjacent positions of alignment are adequately described by transition-state rate theory.

Thus, the rate at which the channel complex advances by one step relative to the rotor is given by

$$j_a = p_{-+}\, k_a, \tag{6}$$

where $p_{-+}$ is the fraction of time that the $o$-site is protonated while the $i$-site is empty, and

$$k_a = \nu \exp(-fd/2kT) \tag{7}$$

is the transition rate constant for a step forward. The force in the spring is denoted by $f$, and $d$ is the distance between adjacent binding sites. The frequency factor, $\nu$, depends on the microscopic friction experienced by the channel complex and on the width and height of the activation barrier due to its interaction with the M-ring (Chandrasekhar, 1943). To simplify the formalism, we have assumed that this activation barrier is situated at the midpoint between two positions of alignment, that it is narrow, and that it is larger than $-e\Delta p/2$. We further require that the force in the spring, $f$, vary relatively little over the distance between adjacent proton-accepting sites. Under these conditions, the activation energy for advancing is raised by $fd/2$, which decreases the transition rate constant by the factor $\exp(-fd/2kT)$. Similarly, one finds that the rate at which the channel complex retreats relative to the M-ring is given by

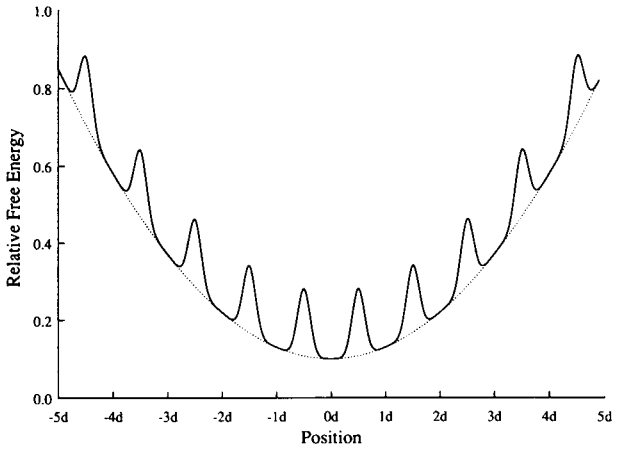


FIGURE 3 The free energy of the channel complex as a function of its position relative to the stator. The broken line illustrates the free energy stored in the elastic linkage. The solid line includes the potential barriers due to interactions with the rotor.

$$j_r = p_{+-}k_r, \tag{8}$$

where $p_{+-}$ is the fraction of time that the $i$-site is protonated while the $o$-site is empty, and

$$k_r = \nu \exp(fd/2kT) \tag{9}$$

is the transition rate constant for a step backward. During steady rotation of the filament, the channel complex must remain stationary relative to the stator. Thus, its net forward stepping rate relative to the rotor, $j_a - j_r$, must equal the rate at which binding sites on the M-ring move past the stator:

$$j_a - j_r = m\Omega, \tag{10}$$

where $m$ is the number of binding sites on the rotor, and $\Omega$ is its rotation rate.

Fig. 4 shows a diagram of all the allowed transitions in the state of the channel complex. The configuration of the two binding sites is denoted by $[io]$, where $i$ and $o$ are either $-$ or $+$, depending on whether the corresponding site is vacant or protonated. Transitions along the periphery of this diagram represent proton transfer to or from a proton-accepting site. Transitions along the diagonal correspond to steps of the channel complex relative to the M-ring. During steady rotation of the filament, the elastic linkage between channel complex and stator is stretched by a fixed amount, and thus the rate constants $k_a$ and $k_r$ do not vary in time. The probabilities, $p_{io}$, of finding the

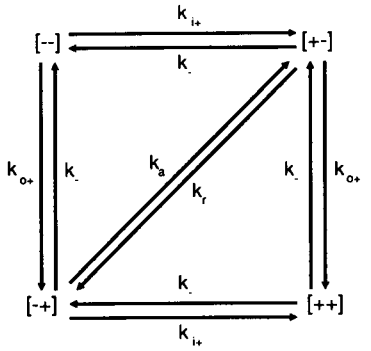


FIGURE 4 Transitions between states of the channel complex during steady rotation of the filament (see text).

channel complex in any of the four states $[io]$ are also constant in time and add up to unity. This results in four independent equations for the four variables, $p_{io}$, that are solved to yield the net stepping rate along the diagonal, $j_a - j_r$, as a function of the rate constants $k_{o+}$, $k_{i+}$, $k_-$, $k_a$, and $k_r$. The torque exerted on the rotor is given by

$$M = nf(md/2\pi), \tag{11}$$

where $n$ is the number of independent channel complexes, and $md/2\pi$ is the radius of the rotor. Inserting Eq. 11 into Eqs. 7 and 9, one obtains the transition rate constants $k_a$ and $k_r$, and consequently the stepping rate, $j_a - j_r$, as a function of the torque exerted on the rotor. Finally, Eq. 10 yields the rotation rate of the motor as

$$\Omega = \frac{\nu}{m} \frac{AW^{-1/2} - RW^{1/2}}{1 + U(BW^{-1/2} + SW^{1/2})}, \tag{12}$$

where

$$W = \exp(2\pi M/nmkT),$$

$$U = \nu/Kh,$$

$$A = \frac{PQ}{(1 + Q)(1 + PQ)}$$

$$R = \frac{Q}{(1 + Q)(1 + PQ)}$$

$$B = \frac{1 + PQ/(1 + Q) + 1/(1 + PQ)}{(1 + Q) + (1 + PQ)}$$

$$S = \frac{1 + 1/(1 + Q) + Q/(1 + PQ)}{(1 + Q) + (1 + PQ)}$$

$$P = \exp(-e\Delta p/kT)$$

and

$$Q = H_i/K.$$

## PROPERTIES OF THE MODEL

Eq. 12 fully describes the behavior of this mechanism during steady rotation. In a subsequent publication, a more general treatment will be given that allows for transient phenomena and includes partial uncoupling. Five independent combinations of parameters characterize any specific version of the model: $\nu/m$ scales the motor's speed; $nm$ scales the motor's torque and determines the rotation-dependent proton flux; $H_i/K$ affects the dependence on the absolute pH of the cytoplasm and the external medium; $\chi$ affects the dependence on the membrane potential; and $\nu/Kh$ determines the relative importance of proton transfer processes and mechanical movement in limiting the motor's rate of rotation. In addition, the rotation rate depends on five external variables accessible to experimental manipulation: the membrane potential, $\Delta\psi$; the pH of the cytoplasm, $pH_{in}$; the pH of the external medium, $pH_{out}$; the temperature, $T$; and the torque exerted on the rotor, $M$.

We restrained our choice of parameters for fits to the experimental measurements by setting the proton binding rate constant to $h = 4 \times 10^{11}\ M^{-1}s^{-1}$, the value measured for a proton binding site in a calcium channel by Prod'hom et al. (1987). Furthermore, we fixed the number of channel complexes as $n = 8$, corresponding to the number of independent torque generators observed in recent experiments by Blair and Berg (1988). The frac-

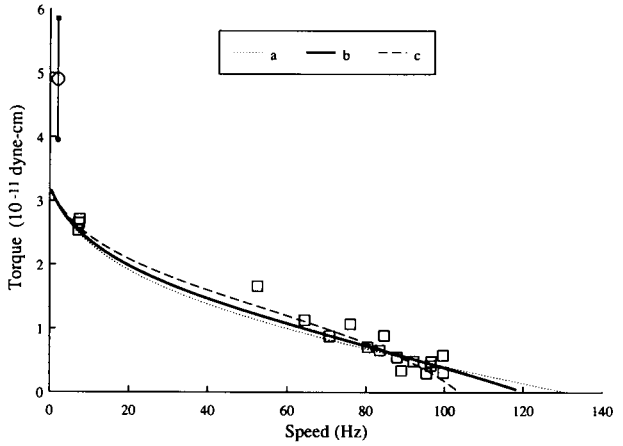


FIGURE 5 The torque generated by the flagellar motor as a function of its rotation rate. The measurements of Lowe et al. (1987) are plotted with square symbols. The curves are calculated from our model using the following parameter sets (a) $pK = 7.1$, $\nu = 3.3 \times 10^4\ s^{-1}$, $m = 105$; (b) $pK = 7.3$, $\nu = 5 \times 10^4\ s^{-1}$, $m = 105$; (c) $pK = 7.5$, $\nu = 2 \times 10^5\ s^{-1}$, $m = 105$. The external variables are $\Delta p = -150$ mV, $pH_{in} = 7.3$, $pH_{out} = 7.5$, and $T = 22$°C. The stall torque predicted from the measurements of rotation-dependent proton flux is plotted with a circular symbol.

tional transmembrane electrical distance between the cytoplasm and the proton-accepting sites was set to $\chi = 0.5$. These choices leave only three free parameters: $K$, $\nu$, and $m$.

Figs. 5–7 summarize the model's predictions for experimental observations that will be discussed in the following sections. Three sets of values for $K$, $\nu$, and $m$ were chosen that gave acceptable fits to the torque-speed diagram, Fig. 5. We will refer to these sets as (a), (b), and (c), respectively.

## Stall torque

At vanishing speed, the numerator in Eq. 12 vanishes, and our mechanism generates a torque,

$$M_0 = kT(nm/2\pi)\ ln\ W = (-e\Delta p)\ nm/2\pi. \qquad (13)$$

This stall torque is directly proportional to the protonmotive force, $\Delta p$, and to the number of protons transferred per revolution, $nm$. No other external variables or model-specific quantities affect the stall torque.

We know from experiment that the stall torque of the flagellar motor is very close to the torque developed at the low rotation rates of tethered cells (Meister and Berg, 1987). At a given protonmotive force, this running torque is independent of temperature over the range of 4 to 38°C, in agreement with Eq. 13 (Khan and Berg, 1983). It also shows no deuterium solvent isotope effect, remaining unchanged when tethered cells are shifted from $H_2O$ to $D_2O$ (Khan and Berg, 1983). Finally, studies using artificially induced proton gradients have shown that the torque developed in tethered cells varies proportionally with the protonmotive force, at least up to a value of −80 mV (Manson et al. 1980; Conley and Berg, 1984; Khan et al., 1985). The apparent saturation of the stall torque at higher protonmotive force might actually reflect failure of the methods for artificially energizing cells in that regime. In fact, there is evidence for an increase in torque proportional to $\Delta p$ up to the value of $\sim -150$ mV generated by metabolizing cells (Meister and Berg, 1987). Lowe et al. (1987) measured the torque of these cells as $2.7 \times 10^{-11}$ dyn cm. As shown in Fig. 5, a value of $nm$ = 840 protons/revolution fits these measurements quite well.

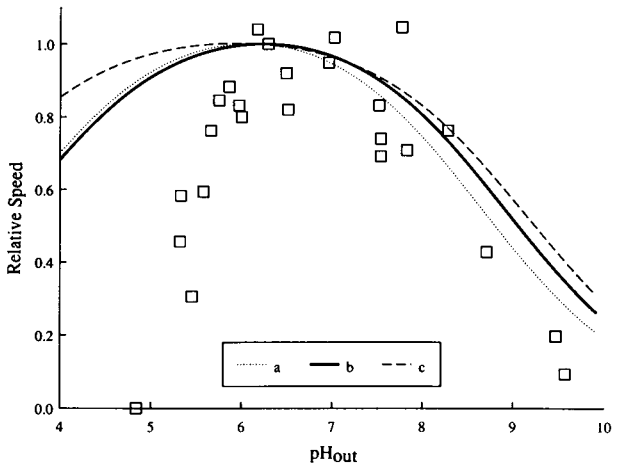


FIGURE 6 The zero-load speed of the flagellar motor as a function of external pH, normalized by its maximal value. The measurements of Shioi et al. (1980) were normalized by the maximal swimming speed of 35 μm/s and plotted with solid symbols. The curves are calculated using the parameter sets and external variables of Fig. 5, except for $T$ = 30°C, and a change in pK of −0.24 for each curve to take account of the higher temperature.

Eq. 13 holds for any tightly coupled motor. Consider a motor mechanism which transfers a constant number of protons, $s$, for each revolution of the flagellar filament. When rotation of the filament is stalled by an external torque, no protons can flow through the motor. Because the protonmotive force and the external torque are the only thermodynamic driving forces acting on the system, one concludes that no dissipation of free energy occurs at stall. The stalled motor is in thermodynamic equilibrium; in the language of irreversible thermodynamics, this state is referred to as "static head" (Kedem and Caplan, 1965). During infinitesimally slow rotation close to stall, the motor operates reversibly, that is, with unit efficiency. Thus, the free energy lost during each revolution by the protons traversing the motor is equal to the mechanical work performed by the filament in its rotation against the stall torque:

$$s(-e\Delta p) = 2\pi M_0. \qquad (14)$$

This is equivalent to Eq. 13, where $s = nm$. Clearly, the dynamical details of a tightly coupled motor are irrelevant to its stall torque. The latter is an equilibrium property that depends exclusively on the protonmotive force and the stoichiometry of protons to revolutions.

## Speed at zero load

The motor attains its maximum speed, $\Omega_o$, when it generates no torque. At this point, $W = 1$ in Eq. 12, and our model predicts

$$\Omega_o = \frac{\nu}{m}\frac{A - R}{1 + U(B + S)}. \qquad (15)$$

Note that this value is independent of the parameter combination $nm$. If $U = \nu/Kh \ll 1$, the motor's rotation rate is limited only by the mobility of the channel complex, and

$$\Omega_o \xrightarrow[U\to 0]{} \frac{\nu}{m}\frac{Q(P - 1)}{(1 + PQ)(1 + Q)}. \qquad (16)$$

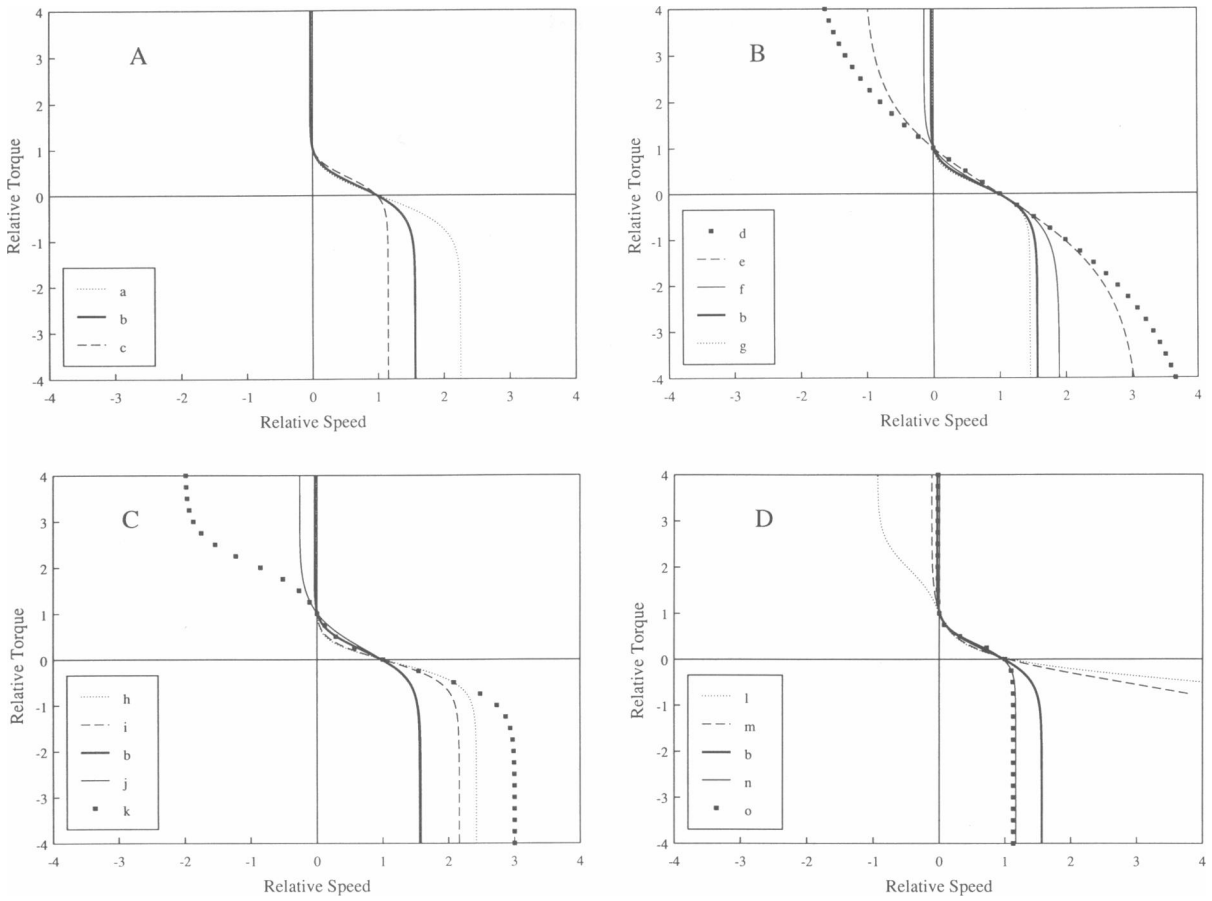


FIGURE 7 The torque generated by the model mechanism as a function of the rotation rate. Torque and speed are normalized by the stall torque and the zero-load speed, respectively. (*A*) Torque-speed relationships for the parameter sets used in Fig. 5. $P = 403$ for all curves. (a) $Q = 0.0250$, $U = 1.039$; (b) $Q = 0.0395$, $U = 2.494$; (c) $Q = 0.0627$, $U = 15.81$. The remaining panels show the torque-speed relationships for extended parameter sets, with curve (b) included for reference. (*B*) Variation of $P$ (i.e., of protonmotive force in steps of ~60 mV). $Q = 0.0395$ and $U = 2.49$ for all curves. $P = 0.403$ (d), 4.03 (e), 40.3 (f), 403 (b), 4,030 (g). (*C*) Variation of $Q$ (i.e., of $pK$-$pH_i$ in steps of 1 unit). $P = 403$ and $U = 2.49$ for all curves. $Q = 0.000395$ (h), 0.00395 (i), 0.0395 (b), 0.395 (j), 3.95 (k). (*D*) Variation of $U$ (i.e., of the ratio of the stepping rate to proton dissociation rate by factors of 10). $P = 403$ and $Q = 0.0395$ for all curves. $U = 0.0249$ (l), 0.249 (m), 2.49 (b), 24.9 (n), 249 (o).

In the extreme of very large $U$, proton binding and release are rate-limiting, and

$$\Omega_o \xrightarrow[U\to\infty]{} \frac{Kh}{m}\frac{Q(P-1)}{2+Q(P+1)}. \qquad (17)$$

Experimentally, it is known that the motors of swimming cells rotate at close to the zero-load speed (Lowe et al., 1987). Their rotation rate decreases by a factor of 1.5–2 when $H_2O$ is replaced by $D_2O$ in the surrounding medium (Lowe, 1987). This is an indication that proton transfer processes are at least partly responsible for limiting the zero-load speed of the motor. Many weak acids show a pK for binding of deuterons about 0.4–0.6 units above the pK for binding of protons (Laughton and Robertson, 1969). Prod'hom et al. (1987) saw an isotope-dependent shift of 0.35 units in the pK for the binding of hydrogen ions to a site in a calcium channel. They noted that the change results from a decrease in the dissociation rate, while the association rate constant, $h$, varies little under isotope exchange. Consequently, we modeled the deuterium isotope effect on the motor as an increase in pK by 0.4 units. With the parameter sets (a), (b), and (c) of Fig. 5 one calculates a deuterium isotope effect on the zero-load speed of 1.7, 1.8, and 2.0, respectively.

The rotation rate of the motor in swimming cells is strongly temperature-dependent. Lowe et al. (1987) found that it increases by a factor of 2.4 between 16 and 32°C. Quantities that one would expect to be temperature dependent in our expression for the zero-load speed, Eq. 15, are $\nu$, $K$, and $h$. Many amino acids show a shift in the pK for proton binding with temperature of ~0.03 per degree centigrade (King, 1965). If one ascribes the temperature dependence of the zero-load speed exclusively to

this change in pK, our model predicts an increase between 16 and 32°C by a factor of 1.5, 1.7, and 1.9, using parameter sets (a), (b), and (c), respectively. It is plausible that the mobility of the channel complex, $\nu$, which is limited by transitions over large potential barriers, is also thermally activated. The models described by parameter sets (b) and (c) are primarily limited by proton transfer processes ($U = 2.5$ and 15.8, respectively), and their zero-load speed depends only weakly on the value of $\nu$. On the other hand, using parameter set (a) ($U = 1.04$), an activation enthalpy for $\nu$ of 40 $kT$ (roughly 24 kcal/mol) would by itself be sufficient to predict the observed temperature effects.

Shioi et al. (1980) reported a decrease in the swimming speed of *Bacillus subtilis* at pH values below 6 and above 8. The bacteria in this study had a cytoplasmic pH of ~7.3 and a protonmotive force of $\sim -150$ mV, which varied little as the external pH was changed. Thus, only the relative contribution of $\Delta\psi$ to the protonmotive force was altered during the experiment. Our model predicts a change in the zero-load speed under these conditions only if the proton-binding sites are electrically separated from the cytoplasm (i.e., if $\chi > 0$), in which case the proton concentration at the $i$-site, $H_i$, varies with $\Delta\psi$. Fig. 6 shows the zero-load speed of this mechanism as a function of external pH and compares it to the measurements of Shioi et al. (1980). Although the model roughly predicts the $pH_{out}$ at which the bacteria swim fastest, it fails to explain the rapid decrease in motility at low $pH_{out}$. A perfect fit can be obtained if $\chi$ is chosen as 0.8 and $h$ is set to $4 \times 10^{12}$ $M^{-1}s^{-1}$, but the latter value seems somewhat large. On the other hand, extreme values of $pH_{out}$ may have other effects on the motile apparatus. For example, changes in the shape of various proteins may alter the mobility of the channel complex, or the strength of the coupling constraints, or even the structure of the flagellar filament (Kamiya et al., 1982).

## Relationship between torque and speed

Fig. 5 illustrates how the torque generated by this model mechanism varies with the rate of rotation and compares its behavior to the measurements of Lowe et al. (1987). Fits of similar quality can be obtained with a variety of different parameter sets, and curves (a) and (c) merely show two extremes of the acceptable range. Note that the parameter sets (a), (b), and (c) all make roughly correct predictions regarding the deuterium isotope effect and temperature dependence discussed above. Thus, the current empirical knowledge leaves considerable quantitative uncertainty about the various ingredients of our model. In particular, the parameter $U = \nu/Kh$, which reveals the relative roles of proton transfer and mechanical motion in limiting the motor's speed, ranges from 1.0 to 15.8 for the three curves in Fig. 5.

During its normal operation, the flagellar motor drives a passive viscous load. Thus its torque never changes sign (unless the sensory system switches the motor's sense of rotation), and it never exceeds the stall torque. However, it is possible experimentally to apply a positive torque greater than the stall torque, which will drive the motor backwards, i.e., at negative speed, contrary to its natural direction of rotation. Under these conditions, the motor acts as an ion pump, moving protons up their potential gradient. Another experimental possibility is to apply a negative torque, one that will accelerate the motor in a positive direction, i.e., in its natural direction of rotation. By this means, the speed of the motor can be made greater than the zero-load speed. It is of interest to study the properties of our model in these regimes. At the extremes of very large positive or negative torque, one finds that the speed approaches a maximal value of

$$\Omega \xrightarrow[M \to +\infty]{} -\frac{Kh}{m}\frac{R}{S} \tag{18}$$

or

$$\Omega \xrightarrow[M \to -\infty]{} \frac{Kh}{m}\frac{A}{B}. \tag{19}$$

These limits are determined by the proton transfer rates, not by the mobility of the channel complex, because the transition rate constants for stepping, $k_r$ or $k_a$, can be increased arbitrarily by applying a large torque. $Kh$ is the rate at which an occupied site dissociates and $m$ is the number of these events per revolution, so that $Kh/m$ is the upper limit imposed by dissociation. The factors $R/S$ and $A/B$, which are always smaller than unity, reflect the additional time required for association of protons with unoccupied sites.

Torque-speed diagrams for the intermediate range are shown in Fig. 7. The shapes of these curves depend exclusively on the quantities $P = \exp(-e\Delta p/kT)$, $Q = H_i/K$, and $U = \nu/Kh$, whereas the quantities $\nu/m$ and $nm$ act only by scaling the curve along the two axes (Eq. 12). Therefore, we have plotted torque and speed relative to the values of stall torque and zero-load speed, respectively. Fig. 7 *A* shows the behavior expected for the parameter sets (a), (b), and (c). The model predicts that the torque required to drive the motor backwards or to raise its speed beyond the zero-load value should increase steeply. In addition, the speed should saturate at an external torque comparable in magnitude to the stall torque. Note that the value of the maximal speed could discriminate between the parameter sets (a), (b), and (c), and, more generally, between models of different $U$. To examine the behavior of the motor over a wider range of

parameters, we started with the values of set (b) and varied $P$, $Q$, or $U$ independently by factors of 10, as shown in Fig. 7, *B–D*. The torque-speed relationship is most sensitive to these parameters at rotation rates that are negative or larger than the zero-load value. Thus, studies at large externally applied torques would be helpful in determining the relative importance of proton transfer processes and macromolecular motions in the flagellar motor.

## Proton flux through the motor

In any tightly coupled mechanism, the rate of proton translocation through the motor, $J$, is strictly proportional to its rotation rate,

$$J = s\Omega = nm\Omega. \quad (20)$$

Meister et al. (1987) measured the component of the total proton flux across the *Streptococcus* membrane that is coupled to flagellar rotation. They found that, in fact, the ratio of flux to rotation rate remained constant over a wide range of speeds and under varying conditions of protonmotive force, temperature, or hydrogen isotope. Using their estimate of the stoichiometry, $nm = 1{,}240 \pm 240$ protons/revolution, and Eq. 14 (which follows from the assumption of tight coupling), one predicts a stall torque of $(4.90 \pm 0.95) \times 10^{-11}$ dyn cm. This value also is plotted in Fig. 5. Assuming an uncertainty of 30% in the calculation of drag coefficients by Lowe et al. (1987), the measurements of rotation-dependent proton flux and stall torque are seen to be consistent with our hypothesis of tight coupling.

## CONCLUSIONS

We have presented a simple hypothetical mechanism which exhibits many of the known properties of the flagellar motor. Some of these features follow from the single assumption of tight coupling between flagellar rotation and proton transfer, irrespective of the dynamical behavior of the mechanism which accomplishes this coupling. Any model mechanism that transfers a fixed number of protons per revolution will adequately predict (*a*) the proportionality between the rotation-dependent transmembrane proton flux and the motor's speed, (*b*) the proportionality between stall torque and protonmotive force, and (*c*) the fact that the stall torque is independent of the temperature and the hydrogen isotope in the medium.

The first property is implicit in the assumption of tight coupling, while the second and third follow from the fact that the stalled motor operates at thermodynamic equilibrium (Eq. 14). The observed values for the proportionality constants in (*a*) and (*b*) require a coupling ratio of ~800 protons per revolution. It should be emphasized that all of these features might also be incorporated into a loosely-coupled model of the motor (i.e., one that allows significant slip between the movement of protons and that of the filament; for example, see Oosawa and Hayashi, 1983), but only by explicit construction. The restriction to tight coupling greatly limits the range of model mechanisms to be considered and facilitates their analysis. For other tightly coupled models, see Läuger (1988). A fundamental prediction of tight coupling is that the stall torque should remain proportional to protonmotive force over the full physiological range. A conclusive test of this proposition would be of great interest.

The dynamical innards of a tightly coupled motor are revealed only at high rotation rates, far from the point of thermodynamic equilibrium. Thus, the choice of specific parameters in our analysis is motivated primarily by exerimental observations near the zero-load speed. Within the framework of our model, they suggest that the M-ring carries 100 binding sites with a dissociation constant of pK 7.3 situated about halfway across the cytoplasmic membrane. But we regard our model primarily as a working hypothesis on which to base further experimental tests. For example, more can be learned by using externally applied torques to drive the motor backwards (at negative speed) or forwards at speeds greater than the zero-load speed.

We thank Steve Block for his extensive aid in programming.

This work was supported in part by a grant from the United States National Science Foundation (DMB8645909). M. Meister is a fellow of the Helen Hay Whitney Foundation. S. R. Caplan is a Visiting Associate at the Rowland Institute for Science.

*Received for publication 25 August 1988 and in final form 12 December 1988.*

## REFERENCES

Berg, H. C. 1974. Dynamic properties of bacterial flagellar motors. *Nature (Lond.)*. 249:77–79.

Berg, H. C., and R. A. Anderson. 1973. Bacteria swim by rotating their flagellar filaments. *Nature (Lond.)*. 245:380–382.

Berg, H. C., and S. Khan. 1983. A model for the flagellar rotary motor. *In* Mobility and Recognition in Cell Biology. H. Sund and C. Veeger, editors. de Gruyter, Berlin. 485–497.

Berg, H. C., M. D. Manson, and M. P. Conley. 1982. Dynamics and energetics of flagellar rotation in bacteria. *Symp. Soc. Exp. Biol.* 35:1–35.

Blair, D. F., and H. C. Berg. 1988. Restoration of torque in defective flagellar motors. *Science (Wash. DC)*. 242:1678–1681.

Block, S. M., and H. C. Berg. 1984. Successive incorporation of force-generating units in the bacterial rotary motor. *Nature (Lond.).* 309:470–472.

Chandrasekhar, S. 1943. Stochastic problems in physics and astronomy. *Rev. Mod. Phys.* 15:1–89.

Conley, M. P., and H. C. Berg. 1984. Chemical modification of *Streptococcus* flagellar motors. *J. Bacteriol.* 158:832–843.

Coulton, J. W., and R. G. E. Murray. 1978. Cell envelope associations of *Aquaspirillum serpens* flagella. *J. Bacteriol.* 136:1047–1049.

DePamphilis, M. L., and J. Adler. 1971. Fine structure and isolation of the hook-basal body complex of flagella from *Escherichia coli* and *Bacillus subtilis*. *J. Bacteriol.* 105:396–407.

Kamiya, R., H. Hotani, and S. Asakura. 1982. Polymorphic transition in bacterial flagella. *Symp. Soc. Exp. Biol.* 35:53–76.

Kashket, E. R. 1985. The proton motive force in bacteria: a critical assessment of methods. *Annu. Rev. Microbiol.* 39:219–242.

Kedem, O., and S. R. Caplan. 1965. Degree of coupling and its relation to efficiency of energy conversion. *Trans. Faraday Soc.* 61:1897–1911.

Khan, S., and H. C. Berg. 1983. Isotope and thermal effects in chemiosmotic coupling to the flagellar motor of *Streptococcus*. *Cell.* 32:913–919.

Khan, S., M. Meister, and H. C. Berg. 1985. Constraints on flagellar rotation. *J. Mol. Biol.* 184:645–656.

Khan, S., M. Dapice, and T. S. Reese. 1988. Effects of *mot* gene expression on the structure of the flagellar motor. *J. Mol. Biol.* 202:575–584.

King, E. J. 1965. Acid-Base Equilibria. Ch. 8. Macmillan Publishing Co., New York.

Läuger, P. 1988. Torque and rotation rate of the bacterial flagellar motor. *Biophys. J.* 53:53–65.

Laughton, P. M., and R. E. Robertson. 1969. Solvent isotope effects for equilibria and reactions. *In* Solute-Solvent Interactions. J. F. Coetzee and C. D. Ritchie, editors. Marcel Dekker, Inc., New York. 399–538.

Lowe, G. 1987. Rotation of bacterial flagella at high frequency. Ph.D. thesis. California Institute of Technology, Pasadena, CA.

Lowe, G., M. Meister, and H. C. Berg. 1987. Rapid rotation of flagellar bundles in swimming bacteria. *Nature (Lond.).* 325:637–640.

Macnab, R. M. 1987*a*. Motility and chemotaxis. *In* Escherichia coli and Salmonella typhimurium: Cellular and Molecular Biology. F. D. Neidhardt, editor. American Society for Microbiology, Washington, DC. 70–83.

Macnab, R. M. 1987*b*. Flagella. *In* Escherichia coli and Salmonella typhimurium: Cellular and Molecular Biology. F. D. Neidhardt, editor. American Society for Microbiology, Washington, DC. 732–759.

Macnab, R. M., and S.-I. Aizawa. Bacterial motility and the bacterial flagellar motor. *Annu. Rev. Biophys. Bioeng.* 13:52–83.

Manson, M. D., P. M. Tedesco, and H. C. Berg. 1980. Energetics of flagellar rotation in bacteria. *J. Mol. Biol.* 138:541–561.

Meister, M. 1987. Studies on flagellar rotation: the angular symmetry, the stall torque, and the proton consumption of the bacterial flagellar motor. Ph. D. thesis. California Institute of Technology, Pasadena, CA.

Meister, M. and H. C. Berg. 1987. The stall torque of the bacterial flagellar motor. *Biophys. J.* 52:413–419.

Meister, M., G. Lowe, and H. C. Berg. 1987. The proton flux through the bacterial flagellar motor. *Cell.* 49:643–650.

Oosawa, F., and S. Hayashi. 1983. Coupling between flagellar motor rotation and proton flux in bacteria. *J. Phys. Soc. Japan.* 52:4019–4028.

Prod'hom, B., D. Pietrobon, and P. Hess. 1987. Direct measurement of proton transfer rates to a group controlling the dihydropyridine-sensitive $Ca^{2+}$ channel. *Nature (Lond.).* 329:243–246.

Shioi, J.-I., S. Matsuura, and Y. Imae. 1980. Quantitative measurements of protonmotive force and motility in *Bacillus subtilis*. *J. Bacteriol.* 144:891–897.

Silverman, M., and M. Simon. 1974. Flagellar rotation and the mechanisms of bacterial motility. *Nature (Lond.).* 249:73–74.

Stewart, R. C., and F. W. Dahlquist. 1987. Molecular components of bacterial chemotaxis. *Chem. Rev.* 87:997–1025.